HHS Public Access

Author manuscript

Nat Cell Biol. Author manuscript; available in PMC 2019 May 05.

Published in final edited form as:

Nat Cell Biol. 2018 December ; 20(12): 1370–1377. doi:10.1038/s41556-018-0228-7.

CLN8 is an ER cargo receptor that regulates lysosome biogenesis

Alberto di Ronza[1], **Lakshya Bajaj**[1], **Jaiprakash Sharma**[1], **Deepthi Sanagasetti**[1], **Parisa Lotfi**[1], **Carolyn Joy Adamski**[1], **John Collette**[2], **Michela Palmieri**[1], **Abdallah Amawi**[1], **Lauren Popp**[3], **Kevin Tommy Chang**[1], **Maria Chiara Meschini**[4], **Hon-Chiu Eastwood Leung**[5], **Laura Segatori**[3], **Alessandro Simonati**[4], **Richard Norman Sifers**[2], **Filippo Maria Santorelli**[6], and **Marco Sardiello**[1]

[1]Department of Molecular and Human Genetics, Baylor College of Medicine, Jan and Dan Duncan Neurological Research Institute, Texas Children's Hospital, Houston, Texas, 77030, USA.

[2]Department of Pathology and Immunology, Baylor College of Medicine, Houston, Texas, 77030, USA.

[3]Departments of Chemical and Biomolecular Engineering, Biochemistry and Cell Biology, and Bioengineering, Rice University, Houston, Texas, 77005, USA.

[4]Department of Neurological and Movement Sciences, University of Verona, Verona, Italy.

[5]Departments of Pediatrics and Molecular and Cellular Biology, Dan Duncan Cancer Center, Baylor College of Medicine, Houston, Texas, 77030, USA.

[6]IRCCS Stella Maris, 56028 Pisa, Italy.

Correspondence and requests for materials should be addressed to M.S. (sardiell@bcm.edu).

Author Contributions: M.S. conceived and supervised the study. A.D.R. and M.S. designed the experiments and analyzed data with the contribution of L.S., A.S. and F.M.S. A.D.R. performed confocal analysis, flow cytometry, cycloheximide assay, qPCR and enzyme assays. A.D.R. and L.B. performed subcellular fractionation. A.D.R. and J.S. performed co-IP experiments. A.D.R., L.B., J.S., D.S., P.L., M.P., A.A., L.P. and M.C.M. performed cloning, cell culture and transfection experiments. A.D.R. and P.L. performed IHC. H-C.E.L. performed LC-MS/MS. M.S. performed co-expression and evolutionary analyses. A.D.R. and M.S. wrote the manuscript with help from M.N.B, H-C.E.L, L.S., A.S. and F.M.S. All authors reviewed and edited the manuscript.

Author information: Reprints and permissions information is available at www.nature.com/reprints.

Data availability

The authors declare that the main data supporting the findings of this study are available within the article and its Supplementary Information files. Source data for Fig. 1, 2, 3, 4, and 5 and Supplementary Fig. 2, 3, 4, and 5 have been provided as Supplementary Table 1. All other data supporting the findings of this study are available from the corresponding author upon request. Mass spectrometry data have been deposited in ProteomeXchange with the primary accession code PXD011066 [http://proteomecentral.proteomexchange.org/cgi/GetDataset?ID=PXD011066]. The GEO accession numbers of the microarray datasets analyzed for the co-expression analysis are the following: GDS1237, GDS1249, GDS1344, GDS1369, GDS1411, GDS1413, GDS1427, GDS1439, GDS1553, GDS1579, GDS1580, GDS1604, GDS1617, GDS1665, GDS1667, GDS1673, GDS1685, GDS1732, GDS1779, GDS1807, GDS1812, GDS1869, GDS1917, GDS1962, GDS1973, GDS1989, GDS2010, GDS2023, GDS2046, GDS2052, GDS2083, GDS2088, GDS2089, GDS2118, GDS2125, GDS2154, GDS2164, GDS2189, GDS2204, GDS2213, GDS2215, GDS2216, GDS2221, GDS2250, GDS2251, GDS2307, GDS2339, GDS2374, GDS2414, GDS2416, GDS2418, GDS2426, GDS2431, GDS2432, GDS2453, GDS2470, GDS2471, GDS2484, GDS2486, GDS2491, GDS2495, GDS2499, GDS2526, GDS2534, GDS2548, GDS2565, GDS2604, GDS2609, GDS2611, GDS2615, GDS2628, GDS2635, GDS2653, GDS2657, GDS2697, GDS2724, GDS2728, GDS2737, GDS2749, GDS2750, GDS2755, GDS2760, GDS2772, GDS2779, GDS2782, GDS2789, GDS2794, GDS2819, GDS2821, GDS2822, GDS2832, GDS2835, GDS2838, GDS2860, GDS2902, GDS2919, GDS2935, GDS2958, GDS2959, GDS3062, GDS3217, GDS3220, GDS3223, GDS651.

The authors declare no financial and non-financial competing interests.

Abstract

Organelle biogenesis requires proper transport of proteins from their site of synthesis to their target subcellular compartment[1–3]. Lysosomal enzymes are synthesized in the endoplasmic reticulum (ER) and traffic through the Golgi complex before being transferred to the endolysosomal system[4–6], but how they are transferred from the ER to the Golgi is unknown. Here we show that ER-to-Golgi transfer of lysosomal enzymes requires CLN8, an ER-associated membrane protein whose loss of function leads to the lysosomal storage disorder, Neuronal Ceroid Lipofuscinosis 8 (a type of Batten disease)[7]. ER-to-Golgi trafficking of CLN8 requires interaction with the COPII and COPI machineries via specific export and retrieval signals localized in the cytosolic C-terminus of CLN8. CLN8 deficiency leads to depletion of soluble enzymes in the lysosome, thus impairing lysosome biogenesis. Binding to lysosomal enzymes requires CLN8's second luminal loop and is abolished by some disease-causing mutations within this region. Our data establish an unanticipated example of an ER receptor serving the biogenesis of an organelle and suggest that impaired transport of lysosomal enzymes underlies Batten disease caused by mutations in *CLN8*.

Lysosomes play critical roles in the maintenance of cellular homeostasis by degrading and recycling the majority of cellular macromolecules via the autophagic, endocytic and phagocytic programs[4]. Lysosomal digestive functions rely on more than 50 hydrolytic enzymes whose synthesis is coordinated by a genetic program that oversees the cell's catabolic needs[8–10]. Lysosomal enzymes are trafficked to the lysosome in two stages: transport of the newly synthesized proteins from the ER to the Golgi complex, and their subsequent receptor-assisted transfer from the Golgi to endolysosomal compartments[5,6]. How lysosomal enzymes are transported from the ER to the Golgi complex is unknown, and whether or not this process is aided by specific receptors has not been investigated.

Mounting evidence supports the idea that protein cargos require specific cargo receptor systems for proper sorting along the secretory route[11]. We therefore hypothesized that ER exit of lysosomal enzymes is assisted by a dedicated receptor system. To identify and prioritize candidate ER receptors, we analyzed the relationship between the expression of genes encoding human ER-resident proteins (hereafter referred to as ER genes) and that of genes encoding lysosomal enzymes (lysosomal genes). We used sets of expression microarray data from a wide variety of dynamic states following chemical, biological, or genetic perturbation, an established approach for studying lysosomal regulation[8,9]. We found that the expression of ~10% of ER genes correlates with that of lysosomal genes (Fig. 1a), notably including ER genes participating in the maturation of lysosomal proteins such as oligosaccharyltransferase genes, γ-secretase complex genes, and sulfatase modifying factor genes (Supplementary Table 2). Four ER genes with expression correlated to lysosomal genes encode candidate cargo receptors or proteins possibly involved in vesicular transport: *CLN8*, *TMED4*, *TMED9* and *LMF1* (Supplementary Table 2). To determine whether any of these four candidate receptors interacts with lysosomal enzymes, we employed a bimolecular fluorescence complementation (BiFC) system based on a split YFP variant[12]. We generated two libraries of plasmids encoding lysosomal enzymes ($n = 53$) fused either to YFP N-terminal fragment (Y1) or to YFP C-terminal fragment (Y2), respectively, and two libraries of plasmids encoding the four candidate cargo receptors with Y1 or Y2 tags, which

we confirmed localize to the ER (Supplementary Fig. 1a). A DQ-Red BSA assay to measure the proteolytic activity of the lysosome showed that the overexpression of candidate ER cargo receptors did not alter lysosomal degradation capability (Fig. 1b). Confocal microscopy of HeLa cells co-transfected with CLN8, TMED4, TMED9 or LMF1 plasmids and pools of plasmids expressing lysosomal enzymes showed that only the Y2-CLN8 construct consistently interacted with all of the pools (Fig. 1c and Supplementary Fig. 1b). Pairwise co-transfection of Y2-CLN8 with lysosomal enzymes followed by quantification through flow cytometry showed that CLN8 interacted with two-thirds of the lysosomal enzymes but not with non-lysosomal proteins we tested as a control (Fig. 1d, Supplementary Fig. 1c). Co-immunoprecipitation of CLN8-myc followed by immunoblotting confirmed the interactions detected by the BiFC assay (Fig. 1e).

CLN8 is a ubiquitously expressed ER membrane protein of unknown function that forms homodimers[13]. CLN8 deficiency causes a form of neuronal ceroid lipofuscinosis (NCL) or Batten disease (CNL8; OMIM 600143), a fatal neurodegenerative disorder in which lysosomes accumulate ceroid lipopigments[7,14]. It is worth noting that although most lysosomal storage disorders are caused by deficiency of lysosomal enzymes, CLN8 is not in this category.

To determine whether CLN8 is required for proper delivery of lysosomal enzymes, we analyzed the *Cln8*^{mnd} mouse strain, which bears an early frameshift mutation in *Cln8* that causes CLN8 protein deficiency and features resembling those seen in Batten disease[7]. To focus on the primary molecular insult caused by CLN8 deficiency, we analyzed *Cln8*^{mnd} mice at the pre-symptomatic age of two months[15]. We obtained subcellular fractions enriched for lysosomes from the livers of *Cln8*^{mnd} mice (KO) and age-matched wild-type (WT) mice using a Nycodenz gradient (Supplementary Fig. 2a-c). Comparison of lysosome-enriched fractions by liquid chromatography-tandem mass spectrometry (LC-MS/MS) showed that *Cln8*^{mnd} samples had lower levels of lysosomal enzymes than WT samples (Fig. 2a and Supplementary Fig. 2d). Gene set enrichment analysis (GSEA) of proteomic data showed that lysosomal enzymes were specifically depleted in *Cln8*^{mnd} samples (Fig. 2b and Supplementary Table 3), whereas the sets of lysosomal membrane proteins—which are transported to lysosomes via a different route than lysosomal soluble proteins[5]—and mitochondrial matrix proteins (used as a control) showed no overall variation (Supplementary Fig. 2e and Supplementary Tables 4 and 5). Immunoblot analysis confirmed lower levels of tested lysosomal enzymes in the lysosome-enriched fraction from *Cln8*^{mnd} mice (Fig. 2c). Accordingly, the lysosome-enriched fraction from *Cln8*^{mnd} mice showed reduced activity of several tested lysosomal enzymes (Supplementary Fig. 2f). The amounts of transcripts for lysosomal enzymes in the samples from *Cln8*^{mnd} mice, however, were unchanged or slightly increased (Supplementary Fig. 2g), indicating that the reduction of lysosomal enzymes occurs post-transcriptionally. Immunohistochemical analysis of cortical and cerebellar sections from *Cln8*^{mnd} mice confirmed a reduction of enzyme signals (Supplementary Fig. 3a). Confocal microscopy revealed reduction of enzyme signals at lysosomes (Fig. 2d and Supplementary Fig. 3b) and sparse spots of residual enzymes overlapping with the ER (Supplementary Fig. 4a), indicating a maturation defect. Confocal microscopy and immunoblot analyses of fibroblasts derived from patients with mutations in *CLN8* (ref. 16) showed impaired colocalization of TPP1 with the lysosomal marker LAMP1

(Fig. 2e and Supplementary Fig. 4b) and depletion of tested lysosomal enzymes (Supplementary Fig. 4c).

Cargo receptors that traffic from the ER to the Golgi complex can be retrieved to the ER through interaction with COPI, a protein complex that serves as the coatomer of vesicles involved in retrograde transport[17,18]. COPI recognizes a KKXX retrieval signal at the C-terminus of its target cargo receptors[19,20] and mediates a very efficient retrieval that localizes the cargo receptors predominantly to the ER (and only minimally to the Golgi complex)[21,22]. Several lines of evidence indicated that CLN8 is retrieved from the Golgi to the ER in a COPI-dependent manner. First, CLN8 carries a terminal KKXX signal[23] and localizes primarily to the ER (Supplementary Fig. 4d). Second, cell treatment with CBM, a drug that inhibits COPI-mediated vesicular transport and thereby abolishes the retrieval of cargo receptors[24], increased localization of CLN8 to the Golgi complex (Fig. 3a), as did mutating CLN8's KKXX sequence (Fig. 3b)[23]. Third, BiFC and co-IP experiments showed that CLN8 interacts with the COPI complex and this interaction could be disrupted either by mutating CLN8's KKXX signal or by CBM (Fig. 3c-d and Supplementary Fig. 4e). To test whether CLN8 determines the localization of newly synthesized lysosomal enzymes, we took advantage of the fact that in the BiFC assay, interacting proteins form a stable complex[12] whose localization can be monitored by confocal microscopy. Consistent with the above results, mutagenesis of CLN8's KKXX retrieval signal and CBM inhibition of COPI-mediated retrieval each led to increased localization of the enzyme-Y1/Y2-CLN8 complex to the Golgi (Fig. 3e).

We next investigated the association of CLN8 with COPII, the coatomer of vesicles involved in ER-to-Golgi anterograde traffic[25]. COPII interacts with cargo receptors via its Sec24 subunits, which recognize specific cytosolic ER export signals within the cargo receptor protein sequence. The cytosolic tail of CLN8 contains a ^{261}VDWNF^{265} motif that overlaps with the ΦXΦXΦ ER export signal[26]. Lysates derived from HeLa cells expressing myc-tagged Sec24A, Sec24B, Sec24C or Sec24D were subjected to pulldown using the cytosolic tail of CLN8 fused with GST. Immunoblotting revealed interaction of CLN8 with Sec24a and Sec24c; this interaction was abolished by mutations in the ^{261}VDWNF^{265} motif (Fig. 3f and Supplementary Fig. 4f). Mutagenesis of this motif severely diminished Golgi localization of CLN8 with mutated ER retrieval signal (Fig. 3g and Supplementary Fig. 4g), thus confirming that the ^{261}VDWNF^{265} motif is the CLN8's signal for COPII-mediated ER export. Interestingly, this motif is disrupted by a known pathogenic mutation (W263C; http://www.ucl.ac.uk/ncl/).

Metabolic radiolabeling experiments using CLN8-deficient cells obtained by CRISPR/Cas9 genome editing (Supplementary Fig. 5a-b) showed that CLN8 deficiency delays maturation of lysosomal enzymes (Fig. 4a-d), which was rescued by CLN8 re-expression (Supplementary Fig. 5c). Additional experiments showed that CLN8 deficiency leads to faster clearance of lysosomal enzymes (Fig. 4e-g), supporting the notion that lysosomal enzymes have a maturation defect in the absence of CLN8. We tested whether ERAD inhibition would increase the amounts of mature enzymes in *CLN8*$^{-/-}$ cells. Immunoblot and metabolic radiolabeling experiments indicated that ERAD is responsible for the enhanced degradation of lysosomal cargo proteins in the absence of CLN8; ERAD

inhibition, however, did not translate into an increased trafficking and maturation of enzymes in the absence of CLN8 (Supplementary Fig. 5d-e). These data indicated that receptor-mediated transport is critical for the ER exit of these cargo proteins.

CLN8 is a polytopic membrane protein with five transmembrane domains and two lumen-facing loops (Fig. 5a)[27]. To gain insight into the interaction of CLN8 with lysosomal cargo, we analyzed the evolutionary profile of CLN8 and found that the second luminal loop is the most evolutionarily constrained region of CLN8 (Fig. 5c). Out of ~15 pathogenic missense mutations and single amino acid deletions detected in CLN8 patients (http://www.ucl.ac.uk/ncl/), six map within this loop (Fig. 5a, c). We therefore hypothesized that the second luminal loop is involved in CLN8's interaction with lysosomal enzymes. To test this hypothesis, we generated a CLN8 construct lacking the second loop (CLN8ΔL, Fig. 5b) and used it in interaction studies with lysosomal enzymes. We first verified that CLN8ΔL protein co-localizes with full-length CLN8 (Fig. 5d), can traffic to the Golgi (Fig. 5e), and retains BiFC competence (Fig. 5f). Subsequent pairwise BiFC analyses showed that deletion of the second CLN8 loop disrupted the interaction with tested lysosomal enzymes (Fig. 5g, h). Next, we tested by BiFC/flow cytometry the effects of five pathogenic mutations mapped in the second loop and found that four out of five severely reduced the interaction with lysosomal cargos (Fig. 5i, j). The second luminal loop of CLN8 is thus necessary for CLN8 interaction with lysosomal enzymes, and some CLN8 pathogenic mutations disrupt these interactions.

Our results reveal an unanticipated mechanism for maturation of lysosomal enzymes that requires a specific receptor, CLN8, to transport them from the ER to the Golgi complex. This provides an example of organelle biogenesis that is controlled by an ER cargo receptor. In the absence of CLN8, the trafficking of lysosomal enzymes is disrupted, suggesting that the pathogenesis of Batten disease caused by mutations in *CLN8* is rooted in impaired lysosome biogenesis. A larger implication of our results is that CLN8 control of lysosomal homeostasis could be explored as a potential target for therapeutic intervention in disease conditions, such as certain types of cancer, that are characterized by aberrant or unrestricted lysosomal activation[28,29].

Methods

Molecular biology, cell culture and transfection

cDNA libraries generated by retrotranscription of RNAs from HeLa and HEK293 cells using QuantiTect Reverse Transcription kit were used to PCR-amplify cDNAs for lysosomal proteins and candidate receptors. cDNAs were then inserted in pcDNA3.1[cYFP1], pcDNA3.1[cYFP2], pIND20-inFusion[3XFlag], or pGEX-2T vectors by using the in-Fusion cloning kit (Clontech). CLN8 cDNA was also cloned into the pcDNA3.1/Myc vector (Invitrogen). Oligonucleotides used for InFusion cloning are reported in Supplementary Table 6. pcDNA3[nYFP1-CLN8] and pcDNA3[nYFP2-CLN8] constructs were generated by inserting the signal peptide sequence of calreticulin upstream of the YFP sequence to assure ER import of the constructs and a lumen-facing YFP tag. Cells were grown at 37°C in 5% CO2 in Dulbecco's modified Eagle's medium (Euroclone), supplemented with 1% glutamine and Pen-Strep. HeLa cells and biopsied fibroblasts were grown with 10% and

20% heat-inactivated fetal bovine serum (FBS, Hyclone), respectively. Transfection of full-length cDNAs in HeLa cells was performed by using Lipofectamine LTX Transfection Reagent (Invitrogen), according to the manufacturer's directions. siRNA oligonucleotides were purchased from Thermo Scientific. CLN8 expression was knocked down using ON-TARGETplus SMARTpool (L-013304-00-0010). Non-silencing control siRNA analysis was performed by using ON-TARGETplus Non-targeting Pool (D-001810-10-20). Transfection of siRNAs (50 nM, 24 h after cell plating) in HeLa cells was performed by using Lipofectamine RNAiMAX (Invitrogen) according to the manufacturer's instructions. CLN8dK constructs, CLN8 constructs harboring NCL-related mutations, and glycosylation mutants of CTSD, GALNS and GM2A were obtained by using QuikChange XLII site-directed mutagenesis kit (Invitrogen), according to the manufacturer's directions. CLN8ΔL was obtained by removing codons for amino acids 155–222 using the Q5 Site-Directed Mutagenesis kit (New England Biolabs), according to the manufacturer's directions. The oligonucleotides used for site-directed mutagenesis are reported in Supplementary Table 6. All cells used in this study were not contaminated. The assessment of the contamination was performed by using LookOut® Mycoplasma PCR Detection Kit (Sigma).

Confocal microscopy

Transfected cells were grown on glass coverslips for 24–48 h, washed with phosphate buffered saline (PBS) and fixed with 4% paraformaldehyde (PFA; Sigma-Aldrich) for 15 min. After quenching PFA with 50 mM NH_4Cl for 15 min, cells were washed with PBS and permeabilized in blocking buffer (0.1% saponin/10% FBS in PBS) for 1 hr. Coverslips were then incubated O/N with appropriate primary antibodies and for 1 h with Alexa-Fluor conjugated secondary antibodies (Supplementary Table 7). Coverslips were mounted on glass slides with Vectashield DAPI (Vector Laboratories). Images were taken with Leica TCS SP2 AOBS confocal microscope by using a Plan-Neofluar 20° or 63°ø immersion objective (Carl Zeiss, Inc.). For quantitative co-localization analysis of BiFC interactions with organellar markers, ten independent pictures were acquired and analyzed with Coloc2 plugin in Fiji software. Confocal microscopy analyses of mice brain and human fibroblasts were performed by using AlexaFluor 633 (far-red) in order to avoid overlap with autofluorescent ceroid lipopigments[30]. To quantify lysosomal degradation capacity, cells were incubated with 10 μg/ml of DQ-Red BSA for 24 hours (37°C, 5% CO_2) and subsequently transfected with pcDNA, CLN8-Y2, LMF1-Y2, Y2-TMED4, or Y2-TMED9 for additional 24 hours. Immunostaining to identify transfected cells was carried out with anti-GFP antibody (Supplementary Table 7). Quantification of Corrected Total Cell Fluorescence of DQ-Red BSA signal from GFP-positive cells was performed as previously described[31].

Flow cytometry analysis

HeLa cells were plated in 24-well plates and, after 24 h, transfected with 200 ng YFP1- and 200 ng YFP2-tagged constructs, in combination with 200 ng of Ruby plasmid that was used as a reference for transfection efficiency. After 48 h, the fluorescence of 10,000 cells per sample was determined by flow cytometry using the BD LSRFortessa™ Cell Analyzer (BD Biosciences) with the HTS autosampler device. Only Ruby-positive cells were considered for the subsequent analysis of reconstituted YFP signal quantification.

Generation of CLN8 knock-out cells

CRISPR-Cas9 genome editing was used to introduce a deletion in the *CLN8* gene in HeLa cells, specifically, to delete exon 2, which contains the translation start codon (Supplementary Fig. 5a). To this end, two complementary oligonucleotide couples (Supplementary Table 6), coding for a guide RNA upstream of a proto-spacer adjacent motif (PAM) site in exon 2 of *CLN8* were designed using the online CRISPR design tool (http://crispr.mit.edu). The two oligos were annealed and subsequently cloned into the pX458 plasmid[32], followed by Sanger sequencing of the insert to confirm the correct sequence. HeLa cells were transfected with 2 μg plasmid and split in a 96-well plate by single cell deposition. After 3–4 weeks, DNA was isolated from the expanded single colonies, and used in PCR reactions using oligos to amplify exon 2 of *CLN8* with CloneAmp HiFi PCR Premix (Clontech) according to the manufacturer's instructions; clones unable to produce an amplicon were subsequently Sanger-sequenced to confirm deletion of exon 2. The cells with deletion of *CLN8*'s exon 2 ($CLN8^{-/-}$) were analyzed by Quantitative Real Time PCR to confirm the absence of *CLN8* RNA expression and used for further experiments.

Lentivirus generation, infection and expression

CLN8, GALNS and TPP1 full coding sequences were PCR-amplified and cloned into the pINDUCER20 lentiviral vector by inFusion procedure after removal of the ccdB site and insertion of a 3xFlag cassette and a SalI restriction site were introduced into the vectors' backbone, obtaining the pIND20-CLN8-3xFlag, pIND20-GALNS-3xFlag and the pIND20-TPP1-3xFlag constructs. The oligonucleotides used for CLN8, TPP1 and GALNS cloning into the pINDUCER20 vector are shown in Supplementary Table 6. Lentiviral vectors and their respective packaging vectors (psPAX2 and pMD2G) were cotransfected into HEK293T cells in a 4:3:1 molar ratio, respectively. Media was changed 16 hr following transfection to low volume media (5 mL for a 10 cm dish). Media was collected at 48 hr following transfection, replaced with fresh media (5 mL) and collected again at 72 hr. Viral supernatant was cleared from cell debris via centrifugation (10 min at 4000 rpm) as well as filtration through a 0.45 μM polyethersulfone membrane (VWR). Viruses were added to the receiving cells in complete media with polybrene (8ug/mL) and incubated at 37°C for 48h. Cells were selected for more than a week in geneticin-containing medium (G418, 400 μg/mL). Expression of the transgenes was induced with 2 μg/mL doxycycline.

Co-immunoprecipitation

Cells were lysed in cold NP40 lysis buffer (50 mM Tris-HCl pH 7.5, 150 mM NaCl, 1% NP40, protease and phosphatase inhibitor cocktails). The lysates were precleared by mixing with nonimmune serum and protein G-sepharose beads. The precleared lysates were incubated with appropriate antibodies at 4°C for 1 hr. Protein G-agarose (Roche) was then added to the mixtures and gently rocked for 3 hrs at 4°C. The beads were washed three times with NP40 lysis buffer, and the resulting immunoprecipitates were analyzed by Western blotting.

Western blot analysis

Cells were lysed in cold lysis buffer (20 mM Tris–HCl, pH 7.4, 150 mM NaCl, 1% TritonX-100) in the presence of protease inhibitors (SIGMA) for 30 min on ice. Total protein concentrations were determined by BCA assay (Pierce). Protein samples were separated on Novex® 4–12% Bis-Tris precast Gels (NuPage, Invitrogen) and transferred to Nitrocellulose membranes using the iBLOT transfer system (Invitrogen) according to manufacturer's instruction. Primary and HRP-conjugated secondary antibodies (Supplementary Table 7) were diluted in 5% milk in TBST. Detection was carried out with ECL Western Blotting detection reagent (GE Healthcare). Images were detected with ImageQuant LAS 4000 (GE Healthcare) and quantified by Fiji analysis software.

Binding assay for the interaction of CLN8 with Sec24 proteins

The cytosolic tail of CLN8 (nucleotides 739 to 861 of CLN8's open reading frame) with or without the WdK mutation was amplified from the CLN8-Y2 or CLN8WdK-Y2 construct, respectively, and cloned in pGEX-2T vector, obtaining the GST-CLN8dK and GST-CLN8WdK constructs. The oligonucleotide sequences are reported in Supplementary Table 6. The GST-CLN8dK and GST-CLN8WdK were transformed individually in Rosetta(DE3) cells and protein expression was induced with 0.5 mM IPTG for 4 hours at 37°C. The bacteria were lysed using sonication and 0.5% Triton X-100 in PBS supplemented with complete, EDTA-free protease inhibitor (Roche). The supernatant was then loaded onto a pre-packed column with 1 mL glutathione sepharose 4B (GE healthcare) resin. Elution was performed using a step gradient of 10 mM glutathione in 50 mM Tris-HCl pH 8.0. Fractions with >80% purity were combined and dialyzed overnight in PBS at 4°C. A total of 0.5 μg of purified protein, as determined by OD280 (extinction coefficient calculated using ExPASy ProtParam tool), was incubated overnight at 4°C with 5 μl glutathione sepharose 4B resin (GE healthcare), for each individual experiment. Cell lysates from HeLa cells expressing myc-tagged Sec24A, Sec24B, Sec24C or Sec24D were incubated for 16 hours with GST-CLN8dK or GST-CLN8WdK, immobilized on the resin. Glutathione beads were pelleted and washed three times with NP40 buffer. Sec24 proteins bound to the resin were detected by immunoblotting using the anti-myc antibody.

Cycloheximide assay

CTSD-YFP2 and TPP1-YFP2 constructs were transfected 24 h after *CLN8* siRNA transfection in HeLa cells, and 100 μg/ml cycloheximide (Sigma) were added after 24 hr incubation (corresponding to 48 h after siRNA transfection). Cells were harvested 0, 90, 180 and 270 minutes after treatment for analysis by Western blotting.

Quantitative real-time PCR

RNA samples were obtained using the RNeasy kit (Qiagen) according to the manufacturer's instructions. RNA was quantified using the Nano-Drop 8000 (Thermo Fischer). cDNA was synthesized using QuantiTect Reverse Transcription kit (Qiagen). Real-time quantitative RT-PCR on cDNAs was carried out with iTaq™ Universal SYBR® Green Supermix using C1000 Thermal Cycler detection system (Bio-Rad) with the following conditions: 95ºC, 5min; (95ºC, 10 s; 60ºC, 10 s; 72ºC, 15 s) x 40. For expression studies, the qRT-PCR results

were normalized to an internal control (*Cyclophilin*). Oligonucleotide sequences are reported in Supplementary Table 6.

Mice

The *CLN8*^{mnd} mouse line was purchased from the Jackson Laboratory (specie: C57/B6, strain: B6.KB2-Cln8mnd/MsrJ). All mice used in this study were males and age-matched (2-month old). Mouse studies were approved by the Institutional Animal Care and Use Committee of Baylor College of Medicine and are compliant with all relevant ethical regulations regarding animal research.

Subcellular fractionation

For each sample and replicate, a pool of three mouse livers was centrifuged in a discontinuous Nycodenz (Progen Biotechnik) density gradient as previously described[33], with modifications. Briefly, tissues were homogenized in an assay buffer (0.25 M sucrose, pH 7.2) and centrifuged first at 4,800 X g for 5 min, and then at 17,000 X g for 10 min. The sediment of the second centrifugation was washed at 17,000 X g for 10 min, resuspended 1:1 vol/vol in 84.5% Nycodenz, and placed on the bottom of an Ultraclear (Beckman) tube. On top, a discontinuous gradient of Nycodenz was constructed (layers from bottom to top were: 32.8%, 26.3%, and 19.8% Nycodenz). Samples were then centrifuged for 1 h in an SW 40 Ti rotor (Beckman) at 141,000 X g. Lysosome-enriched fractions were collected from the 26.3/19.8 interface, diluted in 5–10 volumes of assay buffer, and centrifuged at 37000 X g for 15 min. Pellets were resuspended in 500 μl of assay buffer.

LC-MS/MS

An aliquot of two microliters of each sample was quantified using NanoOrange protein quantitation kit (Invitrogen Inc.). All samples were normalized to one microgram per 100 μL with 50 mM ammonium bicarbonate buffer (pH 7.9). The samples were reduced with 100 mM dithiothreitol (BioRad Inc.) in a rotary shaker at 800 rpm at room temperature for 30 min. The reduced cysteine residues were further treated with 400 mM iodoacetamide (Sigma Inc.) in dark at room temperature for 30 min in the same shaker. 40 ng of sequencing grade trypsin (Sigma Inc.) was added to the samples. The digests were added with acetonitrile to 10% final volume. The digestion was allowed to proceed at 37^{o}C for 16 hours with mild shaking. The digestion was stopped by added formic acid to 5% final volume. The tubes were Speedvac dried. The digests were resuspended in 0.1% formic acid and 5% acetonitrile solution. The concentration of digest was measured using NanoOrange. 200 ng of each sample were fed into the Eksigent nanoLC system. The Ekisgent nanoLC and the ABCIEX TripleTOF 5600 mass spectrometer were controlled by the Analyst software version 1.6 (ABCIEX Inc.). The Eksigent nanoLC system had a cHiPLC system. The chips contained a trap column (200 μm × 0.5 mm, ChromXP C18-CL, 3 μm, 120 Å) that trapped the injected peptides in a flow rate of 3 μL/min for 50% 0.1% formic acid and 50% acetonitrile for 5 min at 23^{o}C. The second chip was an analytical column (75 μm × 15 cm, ChromXP C18-CL, 3 μm, 120 Å) with the organic mobile phase gradient set at a 90 min gradient starting from 5 to 35% acetonitrile in 0.1% formic acid in 90 min with a flow rate of 300 nL/min. The acetonitrile concentration was increased to 80% in 5 min. The 80% acetonitrile was kept for 5 min. The final acetonitrile concentration was reduced to 5% within 5 min and then

equilibrated for 20 min for the next sample. The Eksigent nanoLC was linked via the nanoflex to the ABCIEX TripleTOF 5600 mass spectrometer. The spray tip was the PicoTip emitter (360 μm OD, 20 μm ID, 12 cm long with 10 μm tip opening size) from New Objective. The GS 1 gas was set at 3 units and the curtain gas was set at 24 units. The ionization voltage was set at 2400 V. The interface heater temperature was set at 150°C. The MS precursor ions were selected from 400 to 1250 amu. The cycle time was 0.25 second and forty most abundant ions were allowed to pass to the q2 for product ion production. The MS/MS spectra were acquired at 0.1 second at the m/z range of 100 to 2000. Beta-galactosidase tryptic digestion was used as a calibration standard. The raw WIFF files were fed into ProteinPilot software v4.5 (a Paragon-based software, ABCIEX Inc.) for peak generation and database search. The organism was set as mouse and the database was NCBI non-redundant database. GSEA was performed as previously described[34], by searching the indicated lists of proteins in the list of LC-MS/MS-detected proteins ranked from the more abundant to the less abundant in the *Cln8* KO mice compared to WT mice.

Immunohistochemistry (IHC)

Dissected tissues were fixed, immediately after removal, in a 10% buffered formalin solution for a maximum of 24 hr at room temperature before being dehydrated and paraffin-embedded under vacuum conditions. Seven-micrometer sections were deparaffinized in xylene, hydrated in graded alcohols and heated in standard citrate or Tris-EDTA retrieval buffer for 30 min at 95°C. After incubation overnight with the primary antibodies at 4°C, the slides were incubated with biotinylated secondary antibodies (Vector Laboratories Ltd.) for 1 hour at room temperature. Antibody labeling was visualized using the VECTASTAIN ABC kit (Vector Laboratories Ltd.) followed by staining with 3,3'-diaminobenzidine tetrahydrochloride plus (DAB+) according to the manufacturer's instructions (Thermo Scientific) or using the Vector Blue Alkaline Phosphatase Substrate Kit (Vector Laboratories Ltd.).

Metabolic Radiolabeling

Cells were serum-starved in methionine-free media for 1 hr then pulse-labeled with a mixture of ^{35}S-methione and ^{35}S-cysteine for 30 min and chased until collection at the indicated time points. At collection, media samples were gently centrifuged (2500 X g for 5 min) to remove floating cells and transferred to new tubes. Cells were lysed on ice for 30 min in lysis buffer (50 mM Tris-HCl pH 7.4, 150 mM NaCl, 0.5% Nonidet P-40, 1 mM PMSF, 10 mM NaF, 1X protease inhibitor cocktail) and centrifuged at 13,000 rpm for 30 min at 4°C. Supernatants were collected, and mixed with media fractions, primary antibodies and protein G agarose beads, and rotated overnight at 4°C. The next day, beads were stringently washed 4X with lysis buffer. Immunocomplexes were eluted from the beads in 1X sample buffer. After resolution by SDS-PAGE, gels were fixed for 30 min in a 2% salicylic acid, 30% methanol solution and dried before detection with a Typhoon Trio Imager.

ERAD inhibition

For immunoblot experiments, the indicated cell lines were treated with 1 μM MG132 and 1 μM Eeryastatin I for 24 hours prior of protein extraction. For metabolic radiolabeling

experiments, 10 μM MG132 and 6 μM Eeryastatin I were added during the starvation step and kept in the pulse and chase media.

Co-expression and sequence analysis

Expression correlation analysis was performed as previously described[35], with minor modifications. Briefly, 620 genes encoding ER proteins were analyzed by using the g:Sorter tool, which is part of the g:Profiler package[36]. For each selected gene probe, g:Sorter retrieves the probes with the most similar expression profile in a specified GEO data set. The analysis was performed using 104 heterogeneous microarray experiments, based on the HG-U133plus2 GeneChip array. Pairwise probe-to-probe correlation scores were computed as the cumulative occurrence of probes at the top 3% of most correlated gene probes in each dataset. For statistical analysis, gene correlation profiles were compared using the Kolmogorov-Smirnov test. For graphical output, heatmaps were obtained by converting ranks into scores using the formula Score = 100 * $((N_{probes} - rank)/N_{probes})^4$. CLN8 sequence analysis was performed using sequences retrieved from the UCSC Genome Browser (http://genome.ucsc.edu) after recursive BLAT searches in multiple species using available CLN8 protein sequences. The alignment of CLN8 sequences was performed with MULTALIN[37]. Local evolution rates of CLN8 amino acid sequences from mammals, birds, reptiles, amphibians and fishes were estimated using the evolution–structure–function method[38,39]. The accession numbers of the microarray datasets analyzed for the co-expression analysis are provided in the data availability statement below.

Patient Consents

These studies were performed upon receiving informed written consent from the patients or their legal guardians. The study protocol was approved by the ethics committee of the IRCCS Stella Maris, Pisa. All the procedures complied with the requirements of the Declaration of Helsinki.

Statistics and Reproducibility

Sample size for *in-vivo* and *in-vitro* experiments was chosen based on previous studies in order to ensure adequate statistical power. All experiments using cells were performed at least in biological triplicate. Experimental analysis was performed in a blinded fashion for quantification of the Pearson correlation in immunofluorescence analysis. For all other experiments, the analysis was performed in a blinded fashion whenever possible. Randomization together with blinding was used for *in-vivo* IHC analysis. Pre-determined exclusion criteria were used in flow cytometry analysis by determining the efficiency of transfection by quantification of Ruby fluorescence. If efficiency of transfection was not adequate, the data was omitted from the study and sample analysis was repeated. Statistical significance was tested using two-side t-test for simple comparisons, whereas group-level p-values were estimated from the mean z-scores from each individual test. A value of $p < 0.05$ was considered significant. All experimental procedures were reviewed and approved by the Institutional Animal Care and Use Committee at Baylor College of Medicine.

Supplementary Material

Refer to Web version on PubMed Central for supplementary material.

Acknowledgments:

We thank P. Lobel, D. Pearce, J. Cooper, T. Dierks, M. Damme, Z. Liu and S. Elsea for helpful discussion; A. Schiano and M. Rousseaux for technical assistance; H. Zoghbi, R. Sifers, V. Brandt, A. Ballabio, H. Jafar-Nejad, K. Venkatachalam, and M. Wang for critical reading of the manuscript; and B. Turk, K. Yamada, B. Blazar, D. Kohn, T. Beccari and M. Peterfy for providing plasmids encoding lysosomal proteins or other tested proteins. This work was supported by NIH grant NS079618 (to M.S.) and grants from the Beyond Batten Disease Foundation (to M.S.) and the NCL-Stiftung (to M.S.). This project was supported in part by the Hamill Foundation and by IDDRC grant number 1U54 HD083092 from the Eunice Kennedy Shriver National Institute of Child Health & Human Development.

References:

1. Purdue PE & Lazarow PB Peroxisome biogenesis. Annu Rev Cell Dev Biol 17, 701–752, 10.1146/annurev.cellbio.17.1.701 (2001). [PubMed: 11687502]
2. Kornfeld S & Mellman I The biogenesis of lysosomes. Annu Rev Cell Biol 5, 483–525, 10.1146/annurev.cb.05.110189.002411 (1989). [PubMed: 2557062]
3. Chacinska A, Koehler CM, Milenkovic D, Lithgow T & Pfanner N Importing mitochondrial proteins: machineries and mechanisms. Cell 138, 628–644, 10.1016/j.cell.2009.08.005 (2009). [PubMed: 19703392]
4. Luzio JP, Pryor PR & Bright NA Lysosomes: fusion and function. Nature reviews. Molecular cell biology 8, 622–632, 10.1038/nrm2217 (2007). [PubMed: 17637737]
5. Braulke T & Bonifacino JS Sorting of lysosomal proteins. Biochim Biophys Acta 1793, 605–614, 10.1016/j.bbamcr.2008.10.016 (2009). [PubMed: 19046998]
6. Saftig P & Klumperman J Lysosome biogenesis and lysosomal membrane proteins: trafficking meets function. Nat Rev Mol Cell Biol 10, 623–635, 10.1038/nrm2745 (2009). [PubMed: 19672277]
7. Ranta S et al. The neuronal ceroid lipofuscinoses in human EPMR and mnd mutant mice are associated with mutations in CLN8. Nat Genet 23, 233–236, 10.1038/13868 (1999). [PubMed: 10508524]
8. Sardiello M et al. A gene network regulating lysosomal biogenesis and function. Science 325, 473–477, 10.1126/science.1174447 (2009). [PubMed: 19556463]
9. Palmieri M et al. Characterization of the CLEAR network reveals an integrated control of cellular clearance pathways. Hum Mol Genet 20, 3852–3866, 10.1093/hmg/ddr306 (2011). [PubMed: 21752829]
10. Sardiello M Transcription factor EB: from master coordinator of lysosomal pathways to candidate therapeutic target in degenerative storage diseases. Ann N Y Acad Sci 1371, 3–14, 10.1111/nyas.13131 (2016). [PubMed: 27299292]
11. Geva Y & Schuldiner M The back and forth of cargo exit from the endoplasmic reticulum. Curr Biol 24, R130–136, 10.1016/j.cub.2013.12.008 (2014). [PubMed: 24502791]
12. Kerppola TK Design and implementation of bimolecular fluorescence complementation (BiFC) assays for the visualization of protein interactions in living cells. Nat Protoc 1, 1278–1286, 10.1038/nprot.2006.201 (2006). [PubMed: 17406412]
13. Passantino R et al. Identifying protein partners of CLN8, an ER-resident protein involved in neuronal ceroid lipofuscinosis. Biochim Biophys Acta 1833, 529–540, 10.1016/j.bbamcr.2012.10.030 (2013). [PubMed: 23142642]
14. Mole SE, Williams RE & Goebel HH Correlations between genotype, ultrastructural morphology and clinical phenotype in the neuronal ceroid lipofuscinoses. Neurogenetics 6, 107–126, 10.1007/s10048-005-0218-3 (2005). [PubMed: 15965709]
15. Bolivar VJ, Scott Ganus J & Messer A The development of behavioral abnormalities in the motor neuron degeneration (mnd) mouse. Brain research 937, 74–82 (2002). [PubMed: 12020865]

16. Cannelli N et al. Novel mutations in CLN8 in Italian variant late infantile neuronal ceroid lipofuscinosis: Another genetic hit in the Mediterranean. Neurogenetics 7, 111–117, 10.1007/s10048-005-0024-y (2006). [PubMed: 16570191]
17. Letourneur F et al. Coatomer is essential for retrieval of dilysine-tagged proteins to the endoplasmic reticulum. Cell 79, 1199–1207 (1994). [PubMed: 8001155]
18. Bonifacino JS & Lippincott-Schwartz J Coat proteins: shaping membrane transport. Nat Rev Mol Cell Biol 4, 409–414, 10.1038/nrm1099 (2003). [PubMed: 12728274]
19. Ma W & Goldberg J Rules for the recognition of dilysine retrieval motifs by coatomer. EMBO J 32, 926–937, 10.1038/emboj.2013.41 (2013). [PubMed: 23481256]
20. Eugster A et al. Ent5p is required with Ent3p and Vps27p for ubiquitin-dependent protein sorting into the multivesicular body. Mol Biol Cell 15, 3031–3041, 10.1091/mbc.E03-11-0793 (2004). [PubMed: 15107463]
21. Dominguez M et al. gp25L/emp24/p24 protein family members of the cis-Golgi network bind both COP I and II coatomer. The Journal of cell biology 140, 751–765 (1998). [PubMed: 9472029]
22. Emery G, Parton RG, Rojo M & Gruenberg J The trans-membrane protein p25 forms highly specialized domains that regulate membrane composition and dynamics. Journal of cell science 116, 4821–4832, 10.1242/jcs.00802 (2003). [PubMed: 14600267]
23. Lonka L, Kyttala A, Ranta S, Jalanko A & Lehesjoki AE The neuronal ceroid lipofuscinosis CLN8 membrane protein is a resident of the endoplasmic reticulum. Hum Mol Genet 9, 1691–1697 (2000). [PubMed: 10861296]
24. Hu T, Kao CY, Hudson RT, Chen A & Draper RK Inhibition of secretion by 1,3-Cyclohexanebis(methylamine), a dibasic compound that interferes with coatomer function. Molecular biology of the cell 10, 921–933 (1999). [PubMed: 10198047]
25. Kuehn MJ, Herrmann JM & Schekman R COPII-cargo interactions direct protein sorting into ER-derived transport vesicles. Nature 391, 187–190, 10.1038/34438 (1998). [PubMed: 9428766]
26. Otsu W, Kurooka T, Otsuka Y, Sato K & Inaba M A new class of endoplasmic reticulum export signal PhiXPhiXPhi for transmembrane proteins and its selective interaction with Sec24C. J Biol Chem 288, 18521–18532, 10.1074/jbc.M112.443325 (2013). [PubMed: 23658022]
27. Kousi M, Lehesjoki AE & Mole SE Update of the mutation spectrum and clinical correlations of over 360 mutations in eight genes that underlie the neuronal ceroid lipofuscinoses. Hum Mutat 33, 42–63, 10.1002/humu.21624 (2012). [PubMed: 21990111]
28. Hamalisto S & Jaattela M Lysosomes in cancer-living on the edge (of the cell). Curr Opin Cell Biol 39, 69–76, 10.1016/j.ceb.2016.02.009 (2016). [PubMed: 26921697]
29. Perera RM et al. Transcriptional control of autophagy-lysosome function drives pancreatic cancer metabolism. Nature 524, 361–365, 10.1038/nature14587 (2015). [PubMed: 26168401]
30. Seehafer SS & Pearce DA Spectral properties and mechanisms that underlie autofluorescent accumulations in Batten disease. Biochem Biophys Res Commun 382, 247–251, 10.1016/j.bbrc.2009.02.099 (2009). [PubMed: 19248764]
31. Marwaha R & Sharma M DQ-Red BSA Trafficking Assay in Cultured Cells to Assess Cargo Delivery to Lysosomes. Bio Protoc 7, 10.21769/BioProtoc.2571 (2017).
32. Ran FA et al. Genome engineering using the CRISPR-Cas9 system. Nat Protoc 8, 2281–2308, 10.1038/nprot.2013.143 (2013). [PubMed: 24157548]
33. Wattiaux R, Wattiaux-De Coninck S, Ronveaux-dupal MF & Dubois F Isolation of rat liver lysosomes by isopycnic centrifugation in a metrizamide gradient. J Cell Biol 78, 349–368 (1978). [PubMed: 211139]
34. Subramanian A et al. Gene set enrichment analysis: a knowledge-based approach for interpreting genome-wide expression profiles. Proc Natl Acad Sci U S A 102, 15545–15550, 10.1073/pnas.0506580102 (2005). [PubMed: 16199517]
35. Sardiello M et al. A gene network regulating lysosomal biogenesis and function. Science 325, 473–477, 10.1126/science.1174447 (2009). [PubMed: 19556463]
36. Reimand J, Kull M, Peterson H, Hansen J & Vilo J g:Profiler--a web-based toolset for functional profiling of gene lists from large-scale experiments. Nucleic Acids Res 35, W193–200, 10.1093/nar/gkm226 (2007). [PubMed: 17478515]

37. Corpet F Multiple sequence alignment with hierarchical clustering. Nucleic Acids Res 16, 10881–10890 (1988). [PubMed: 2849754]

38. Simon AL, Stone EA & Sidow A Inference of functional regions in proteins by quantification of evolutionary constraints. Proc Natl Acad Sci U S A 99, 2912–2917, 10.1073/pnas.042692299 (2002). [PubMed: 11880638]

39. Spatuzza C et al. Physical and functional characterization of the genetic locus of IBtk, an inhibitor of Bruton's tyrosine kinase: evidence for three protein isoforms of IBtk. Nucleic Acids Res 36, 4402–4416, 10.1093/nar/gkn413 (2008). [PubMed: 18596081]

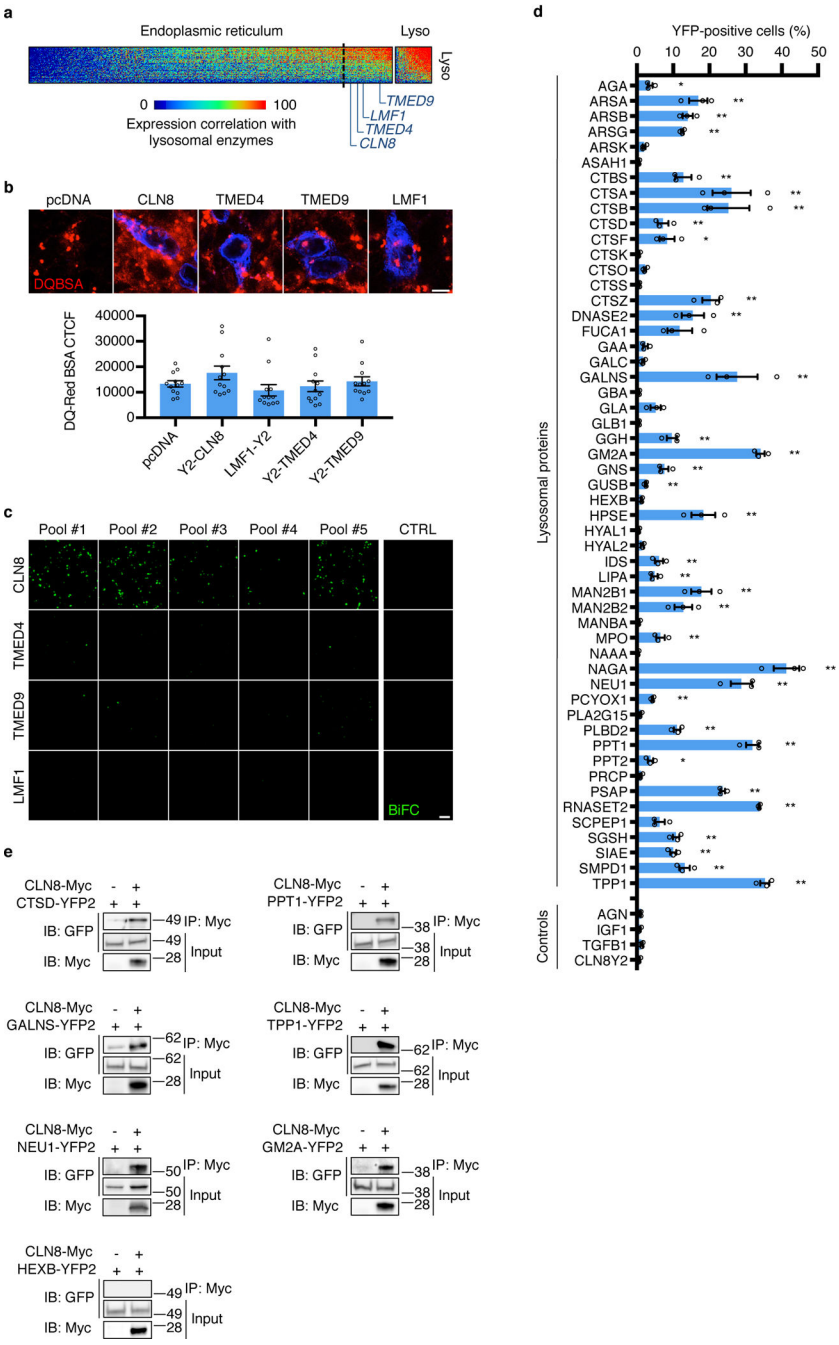

Fig. 1.

CLN8 interacts with lysosomal enzymes. **a**, Co-expression analysis of ER and lysosomal genes. Shown is a heatmap representing the extent of pairwise co-expression between 620 ER genes (*x-axis*) and 60 lysosomal genes (*y-axis*). Among ER genes that are significantly co-expressed with lysosomal genes ($P < 10^{-4}$, two-tailed Kolmogorov-Smirnov test; vertical dotted line), *CLN8*, *TMED4*, *LMF1*, and *TMED9* encode candidate cargo receptors. **b**, DQ-Red BSA degradation assay to measure the proteolytic activity of lysosomes upon transfection of CLN8, TMED4, TMED9 and LMF1 plasmids. CTCF, Corrected Total Cell

Fluorescence. Data are means ± SEM ($n = 3$ independent experiments, $n = 10$ independent images quantified). Scale bar: 20 μm. **c**, Representative live imaging of reconstituted BiFC fluorescence between Y2-tagged, full-length candidate cargo receptors and pools of Y1-tagged lysosomal enzymes. Green fluorescence shows reconstitution of YFP as an indicator of protein-protein interaction. Control experiments (CTRL) were performed by co-transfecting Y2-tagged candidates with pools of Y2-tagged lysosomal enzymes. Scale bar: 200 μm. **d**, Pairwise interaction between Y2-CLN8 and lysosomal enzymes evaluated by BiFC followed by flow cytometry. The non-lysosomal proteins, AGN, IGF1 and TGFB1, and Y2-tagged CLN8 were used as negative controls. Data are means ± SEM ($n = 3$ independent experiments, $*P < 0.05$, **P < 0.01, two-tailed Student's *t*-test). Data are corrected for multiple comparison by using the Bayesian SGoF procedure. **e**, Co-IP analysis of CLN8 and lysosomal enzymes. Proteins were transiently expressed in HeLa cells, and immunoprecipitates were analyzed by immunoblotting with the indicated antibodies. HEXB was used as a negative control. Input represents 10% of the total cell extract used for IP. Images shown in **c** and **e** are representative of $n = 3$ independent experiments.

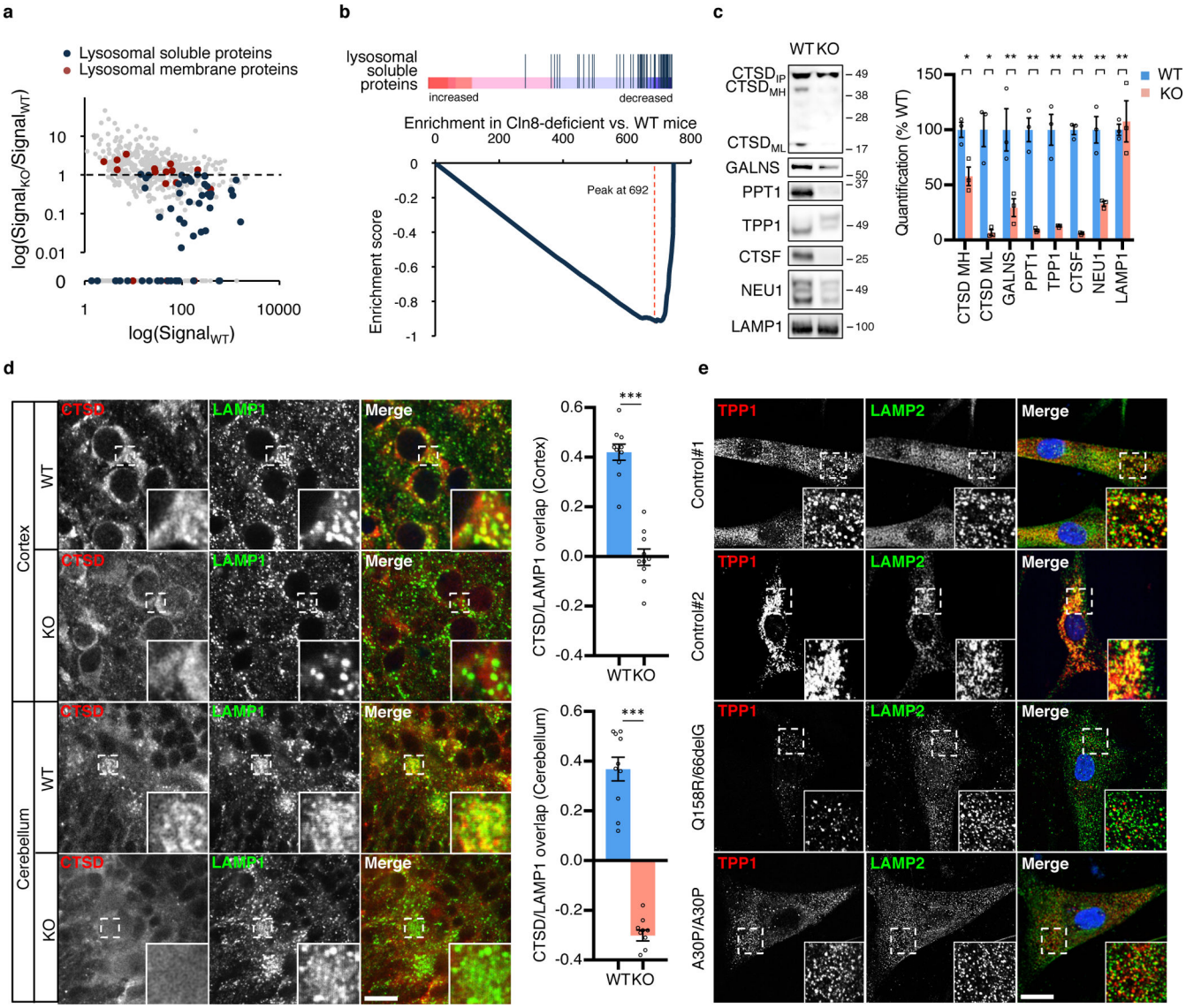

Fig. 2.

CLN8 deficiency leads to depletion of lysosomal enzymes. **a**, Plot of relative protein signals from LC-MS/MS analysis of lysosome-enriched liver fractions from WT and CLN8-deficient mice (KO). Blue dots, lysosomal soluble proteins; red dots, lysosomal membrane proteins; grey dots, other proteins detected by LC-MS/MS. Data are relative to $n = 2$ independent proteomic analyses conducted on pools of three livers each. **b**, GSEA of lysosomal soluble protein changes in CLN8-deficient mice compared with WT mice. The upper graph shows the distribution of lysosomal soluble proteins (vertical blue bars) along the LC-MS/MS-detected proteins ranked according to their enrichment in CLN8-deficient vs. WT mice (left: increased in CLN8-deficient mice, red; right: decreased in CLN8-deficient mice, blue). The lower graph is the enrichment score plot showing that lysosomal soluble proteins rank mostly amongst proteins that are depleted in the CLN8-deficient mice (Enrichment Score = −0.92; $P < 10^{-4}$). **c**, Immunoblot analysis of lysosome-enriched

fractions confirming depletion of lysosomal enzymes in CLN8-deficient mice (KO) compared to WT mice. $CTSD_{IP}$, immature precursor; $CTSD_{MH}$, mature heavy form; $CTSD_{ML}$, mature light form. Band intensities were quantified and normalized to LAMP1. **d**, Confocal microscopy of CTSD (red) and LAMP1 (green) on cortical and cerebellar sections of CLN8-deficient and WT mice. Pearson correlation showed a significant reduction of the CTSD/LAMP1 signal overlap in CLN8-deficient mice compared to WT mice. Inserts show four-fold magnification. **e**, Confocal microscopy of patient-derived CLN8-deficient skin fibroblasts. Skin fibroblasts from two healthy subjects were used as controls. Insets show four-fold magnified images. Quantification is provided in Supplementary Fig. 4b. In **c** data are means ± SEM ($n = 3$ independent experiments, *P < 0.05, **P < 0.01, two-tailed Student's *t*-test). In **d** data are means ± SEM ($n = 3$ independent experiments, $n = 10$ independent images quantified, ***P < 0.001, two-tailed Student's *t*-test). Scale bar: 20 μm.

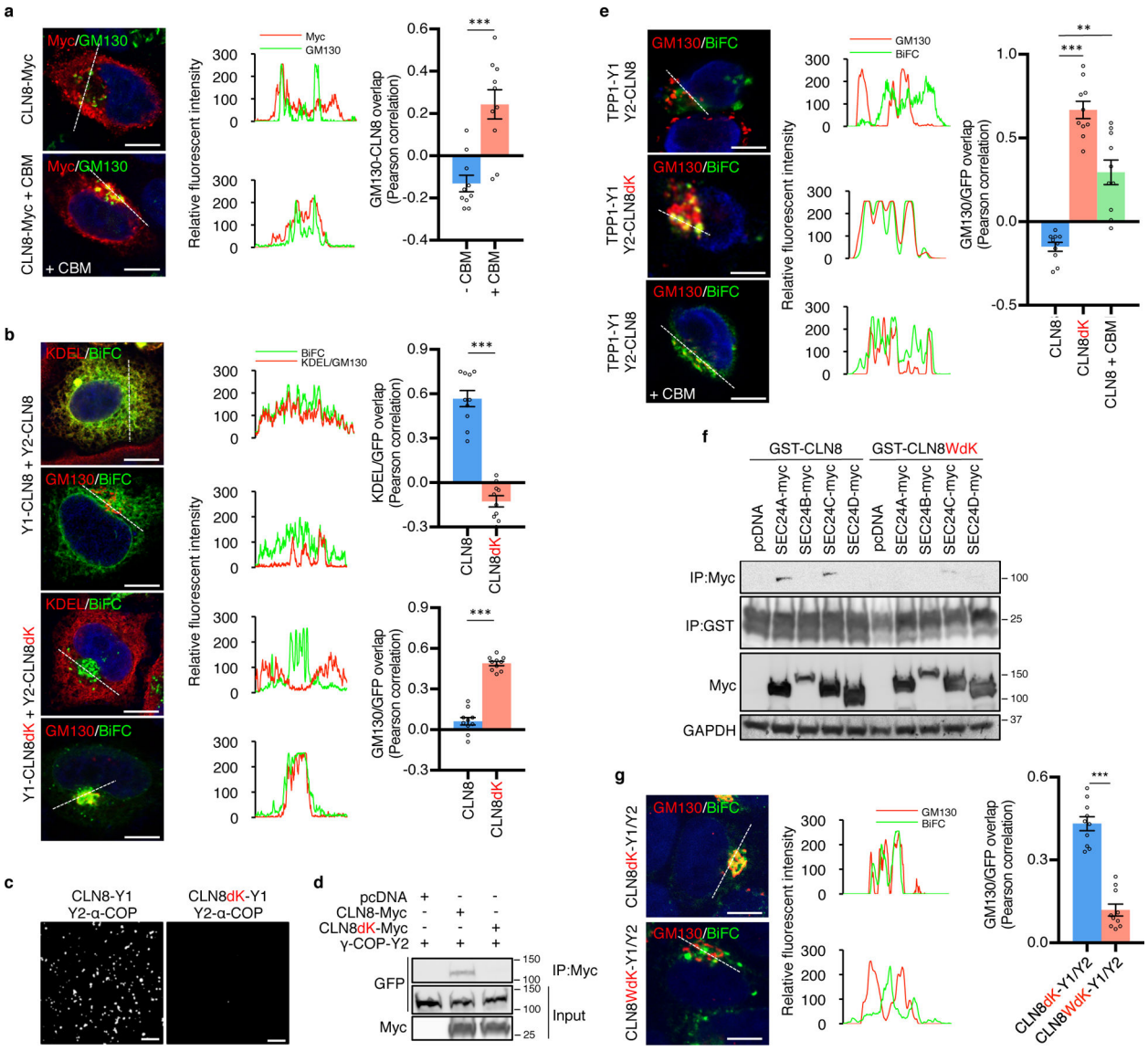

Fig. 3.

Interaction with COPI and COPII complexes mediates CLN8 trafficking. **a**, Confocal microscopy showing ER-to-Golgi shift of CLN8 localization upon treatment with CBM. Trace outline is used for line-scan analysis of Relative Fluorescence Intensity (RFI) of CLN8, GM130 (Golgi marker) and KDEL signals. Signal overlap is quantified by Pearson correlation analysis of $n = 3$ independent experiments, $n = 10$ independent images quantified. **b**, Confocal microscopy of HeLa cells showing ER-to-Golgi shift of CLN8 localization upon KKXX signal mutagenesis (CLN8dK). **c**, BiFC assay of α-COP with CLN8 showing disruption of interaction upon mutagenesis of CLN8's KKXX signal (CLN8dK). **d**, Co-IP assay of γ-COP and CLN8. Input represents 10% of the total cell extract. **e**, Confocal microscopy of BiFC complexes composed of TPP1-Y1 and Y2-CLN8 (with or without CBM) or TPP1-Y1 and Y2-CLN8dk. **f**, Immunoblot of lysates from HeLa cells transfected with Myc-tagged Sec24 proteins after pull down with the cytosolic C-

terminus of CLN8 fused with GST showing disruption of interaction upon mutagenesis of CLN8's COPII signal. **g**, Confocal microscopy of HeLa cells showing decreased Golgi localization of CLN8 upon mutagenesis of CLN8 ER export signal (CLN8WdK) using the Golgi-localizing CLN8dK backbone. In **b**, **e** and **g**, trace outline, RFI and Pearson correlation analyses are performed as in **a**. Images shown in **c**, **d** and **f** are representative of $n = 3$ independent experiments. In **a**, **b**, **e** and **g**, data are means ± SEM ($n = 3$ independent experiments, $n = 10$ independent images quantified, **P < 0.01, ***P < 0.001, two-tailed Student's *t*-test). In **a**, **b**, **e** and **g**, scale bars are 20 μm. In **c**, scale bars are 200 μm.

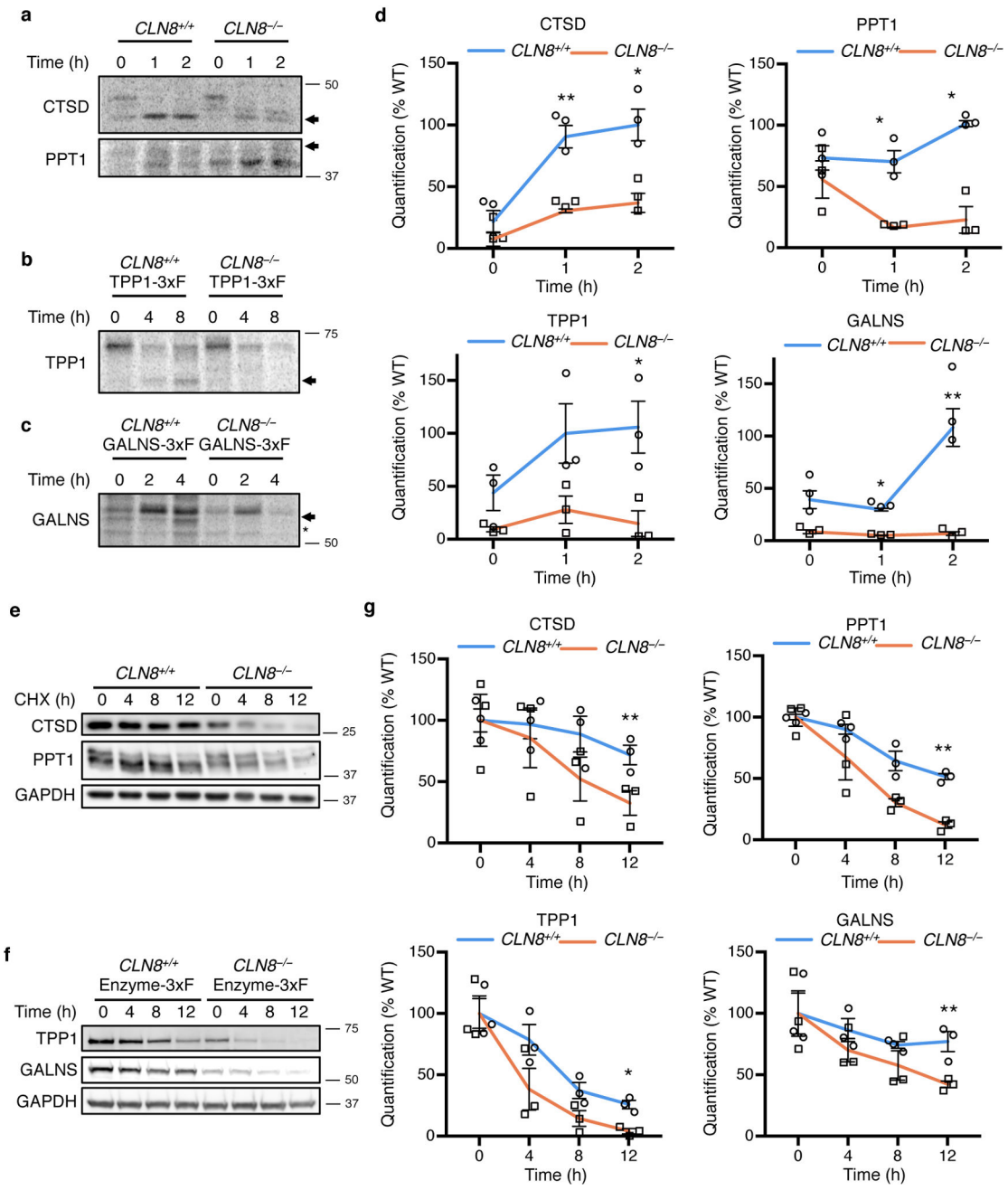

Fig. 4.

Defective maturation of lysosomal enzymes upon CLN8 deficiency. **a-c**, Metabolic radiolabeling of *CLN8*$^{-/-}$ cells and their parental HeLa cells showing defective maturation of CTSD and PPT1 (**a**), TPP1 (**b**) and GALNS (**c**) in the absence of CLN8. CTSD and PPT1 were immunoprecipitated by using antibodies against the endogenous proteins. 3xFlag-tagged TPP1 and GALNS were expressed by using a doxycycline-inducible vector used to transduce *CLN8*$^{-/-}$ and control cells. Arrows indicate the mature, lysosome-associated enzyme. The asterisk in **c** indicates nonspecific signal. **d**, Quantification of the mature

enzymes for metabolic radiolabeling experiment in **a**-**c**. **e**, **f**, Decreased enzyme stability in *CLN8*$^{-/-}$ cells compared to parental HeLa cells. CTSD and PPT1 proteins were monitored at the indicated time points following cycloheximide-mediated blockage of protein synthesis. 3xFlag-tagged TPP1 and GALNS were expressed in cells transduced with a doxycycline-inducible vector and monitored at 0, 4, 8, and 12 hrs upon doxycycline removal to turn off their synthesis. In all experiments, GAPDH was used to normalize the residual protein for quantifications. **g**, Quantification of the immunoblot experiments in **e** and **f**. In **d** and **g**, data are means ± SEM (n = 3 independent experiments, *P < 0.05, **P < 0.01, two-tailed Student's t-test).

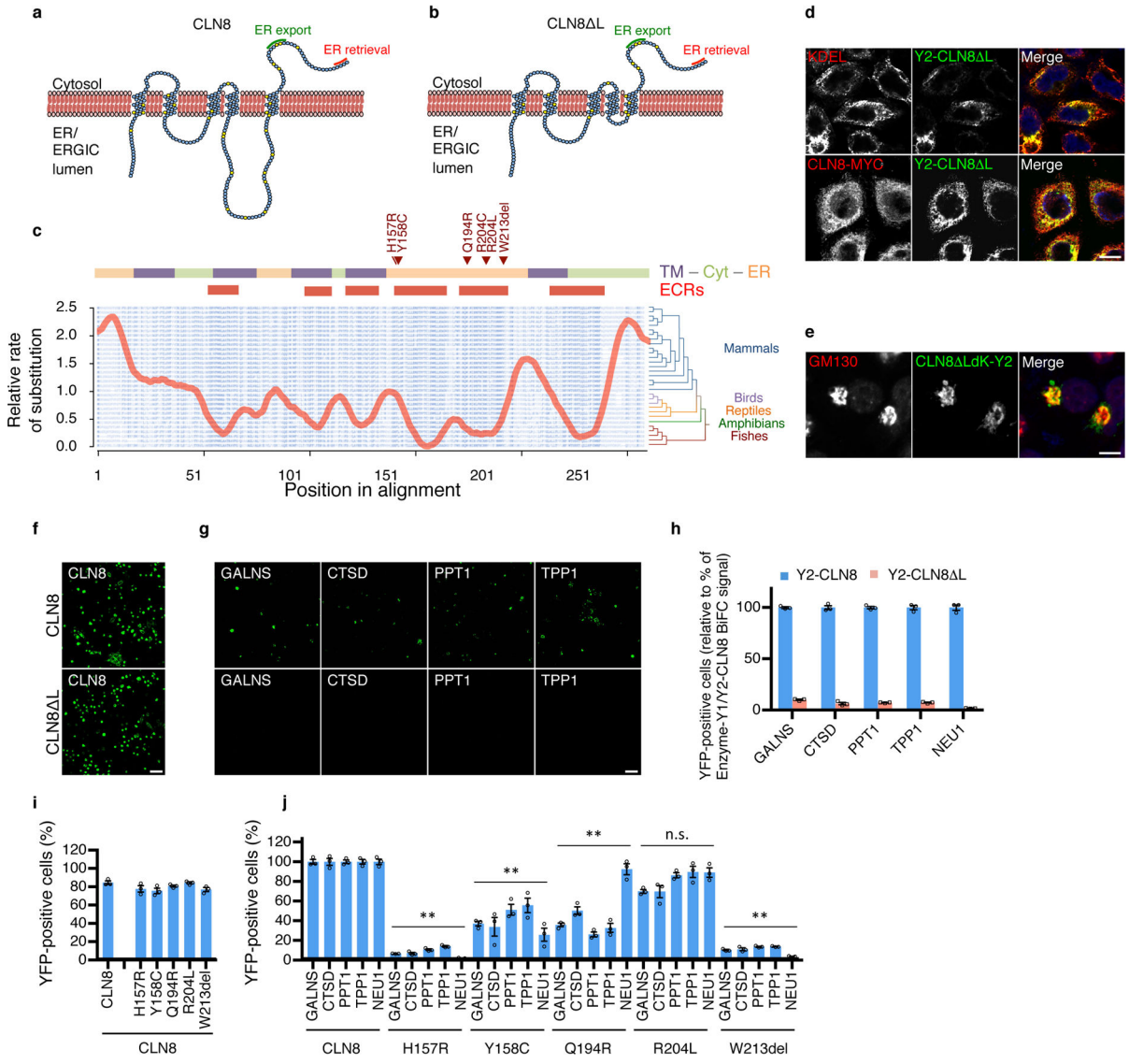

Fig. 5.

CLN8 interaction with lysosomal enzymes requires the second luminal loop. **a**, Schematic representation of CLN8 protein. **b**, Schematic representation of CLN8ΔL construct. Amino acids are represented by colored circles. Amino acids in yellow indicate the position of clinical mutations. The ER export signal and the ER retrieval signal at the protein C-terminus are indicated. **c**, Shown is a multi-alignment of CLN8 protein sequences along with a plot of local evolutionary rates. The red lines at the top mark the detected evolutionary constrained regions (ECRs). Transmembrane domains (TM, purple lines), luminal domains (ER, orange lines) and cytosolic domains (Cyt, green lines) are reported. Clinical mutations that fall in the second luminal loop are reported. **d**, Confocal microscopy analysis showing that Y2-CLN8ΔL co-localizes with both CLN8-Myc and the ER marker, KDEL. Scale bar: 20 μm. **e**, Confocal microscopy analysis showing that mutagenesis of the KKXX signal of the CLN8ΔL-Y protein determines its localization to the Golgi, indicating that the second

luminal loop of CLN8 is not required for CLN8 ER export. **f**, BiFC assay of Y1-CLN8 with Y2-CLN8ΔL showing a reconstituted GFP signal indistinguishable from that of Y1-CLN8 with Y2-CLN8. **g**, Comparative BiFC assay of Y1-tagged lysosomal enzymes with either Y2-CLN8 (top panels) or Y2-CLN8ΔL (bottom panels) showing disruption of interaction upon removal of CLN8 second luminal loop. **h**, Comparative BiFC/flow cytometry analysis of Y1-tagged lysosomal enzymes with Y2-CLN8 or Y2-CLN8ΔL constructs. Values are expressed as a percentage of the enzyme-Y1/Y2-CLN8 interaction. **i**, **j**, Comparative BiFC/flow cytometry assay of CLN8 constructs harboring clinical mutations in the second luminal loop. Images shown in **d**, **e**, **f** and **g** are representative of $n = 3$ independent experiments. In **h**, **i** and **j**, data are means ± SEM ($n = 3$ independent experiments, **P < 0.01, two-tailed Student's *t*-test). In **i** and **j**, the group-level p-values were estimated from the mean z-scores from each individual test. In **d** and **e**, scale bars are 20 μm. In **f** and **g**, scale bars are 200 μm.